LAWRENCE
LIVERMORE
NATIONAL
LABORATORY

LLNL-JRNL-767490

Microbe-embedded Polymer Materials for Selective Rare Earth Recovery

D. M. Park, A. Brewer, Y. Jiao, L. Lammers, E. Chang, D. Reed, A. Dohnalkova, S. Vaithiyalingam, C. Ye

February 6, 2019

Environmental Science and Technology

Disclaimer

This document was prepared as an account of work sponsored by an agency of the United States government. Neither the United States government nor Lawrence Livermore National Security, LLC, nor any of their employees makes any warranty, expressed or implied, or assumes any legal liability or responsibility for the accuracy, completeness, or usefulness of any information, apparatus, product, or process disclosed, or represents that its use would not infringe privately owned rights. Reference herein to any specific commercial product, process, or service by trade name, trademark, manufacturer, or otherwise does not necessarily constitute or imply its endorsement, recommendation, or favoring by the United States government or Lawrence Livermore National Security, LLC. The views and opinions of authors expressed herein do not necessarily state or reflect those of the United States government or Lawrence Livermore National Security, LLC, and shall not be used for advertising or product endorsement purposes.

Microbe Encapsulation for Selective Rare Earth Recovery from Electronic Waste Leachates

Aaron Brewer[1], Alice Dohnalkova[2], Vaithiyalingam Shutthanandan[2], Libor Kovarik[2], Elliot Chang[3], April M. Sawvel[1], Harris E. Mason[1], David Reed[4], Congwang Ye[5], William F. Hynes[5], Laura N. Lammers[3], Dan M Park[1*], Yongqin Jiao[1*]

[1]Physical and Life Science Directorate, Lawrence Livermore National Laboratory, Livermore, California 94550;
[2]Environmental Molecular Sciences Laboratory, Pacific Northwest National Laboratory, Richland, Washington 99354;
[3]Department of Environmental Science, Policy, and Management, University of California Berkeley, Berkeley, California 94270;
[4]Department of Biological and Chemical Processing Department, Idaho National Laboratory, Idaho Falls, Idaho 83415.
[5]Engineering Directorate, Lawrence Livermore National Laboratory, Livermore, California 94550;
*corresponding authors: park36@llnl.gov; jiao1@llnl.gov

Keywords: biosorption, rare earth elements, REE, PEGDA, microencapsulation, NdFeB, electronic waste, microbe beads, continuous flow column

Abstract

Rare earth elements (REEs) are indispensable components of many green technologies and of increasing demand globally. However, refining REEs from raw materials using current technologies is energy intensive and enviromentally damaging. Here we describe the development of a novel biosorption-based flow-through process for selective REE recovery from electronic wastes. An *Escherichia coli* strain previously engineered to display lanthanide binding tags on the cell surface was encapsulated within a permeable polyethylene glycol diacrylate (PEGDA) hydrogel at high cell density using an emulsion process. This microbe bead adsorbent contained a homogenous distribution of cells whose surface functional groups remained accessible and effective for selective REE adsorption. The microbe beads were packed into fixed-bed columns and breakthrough experiments demonstrated effective Nd extraction at a flow velocity up to 3 m/h at pH 4-6. The microbe bead columns were stable for reuse, retaining 85% of the adsorption capacity after nine consecutive adsorption/desorption cycles. A bench-scale breakthrough curve with a NdFeB magnet leachate revealed a two-bed volume increase in breakthrough points for REEs compared to non-REE impurities and 97% REE purity of the adsorbed fraction upon breakthrough. These results demonstrate that the microbe beads are capable of repeatedly separating REEs from non-REE metals in a column system, paving the way for a biomass-based REE recovery system.

TOC

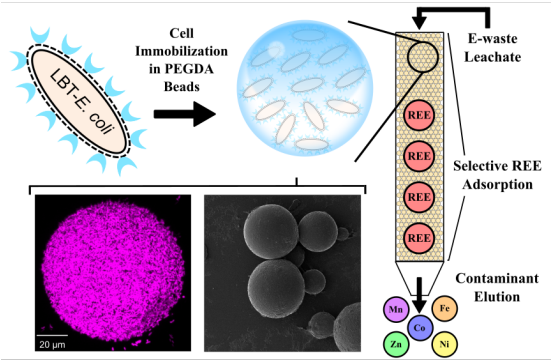

Introduction

The rare earth elements (REEs) are critical components of many clean energy and consumer technologies. As such, the growth of these REE-dependent technologies is expected to significantly increase global REE demand in the coming decades.[1] Despite the presence of significant REE resources worldwide,[2] greater than 80% of the

world's REE supply is from China,[3, 4] leaving global markets vulnerable to supply disruptions.[2, 5] As a result of recent geopolitical tensions, this supply vulnerability has once again been the subject of considerable global attention. One impediment to a more diversified REE supply chain is the difficulty in achieving economical and environmentally sustainable REE extraction and separation from ore deposits and REE-containing waste using current technologies.[6] The environmental burden of current industrial REE production processes is severe[7] due to the generation of radioactive wastes (thorium, and uranium[8]) and high volumes of acidic effluents and organic solvents.[9, 10] To alleviate supply vulnerability and diversify the global REE supply chain, it is imperative to develop new processing methodologies that enable environmentally friendly REE extraction from alternative REE resources.

End-of-life consumer products (e.g. mobile phones, hard drives, hybrid car batteries, phosphors, LED screens, etc.) represent a largely untapped REE source with the potential to bridge the gap between the high industrial demand for critical REEs[11-14] (i.e., Y, Nd, Eu, Tb, Dy [15]) and their low relative abundance in carbonatite deposits, which dominate the REE supply.[2] An additional advantage of REE recycling over ore mining is the reduction in radioactive waste generation given the lack of thorium and uranium in these end-of-life products.[13] However, less than 1% of REEs used today are recycled given the challenge of collection and low efficiencies and limitations in recycling processes.[4, 13] As such, processes that enable efficient and sustainable REE recovery from end-of-life products could help meet the growing demand for critical REEs while addressing the increasing environmental concerns.

Compared to conventional liquid-liquid extraction methods that require a large volume of solvent, solid phase adsorption offers increased energy efficiency as well as reduced solvent consumption.[16] Traditional adsorbents such as silica gels and activated carbon have gained attention as solid phase extractants, owing to their high surface area and abundant negatively charged functional groups.[16-20] Microbe-based adsorptive materials offer similar advantages for solid-phase REE extraction, with potential for environmentally sustainable and economically favorable development.[21] Microorganisms naturally synthesize and display high-density surface-accessible functional groups (e.g., carboxylates and phosphates) as they grow and multiply,[22] facilitating high-capacity REE adsorption without requiring the chemical synthesis steps necessary for producing synthetic extractants. Native microbial surfaces exhibit a general adsorption preference for REEs over most non-REE metal ions,[23-26] and the

surface-adsorbed REEs can be readily recovered through desorption using a targeted eluent such as citrate,[27-29] enabling REE recovery and biomass re-use. Biosorption techniques can be further improved using genetic engineering approaches to rationally modify the cell surface functional groups. For example, altering the cell wall components in *Bacillus subtilis* through targeted gene deletions enhanced the selectivity differences among REEs.[30] Additionally, engineering *Caulobacter crescentus* and *Escherichia coli (E. coli)* to express and display lanthanide binding peptides (LBT)[27, 28] at high densities on the cell surface or on extracellular curli fibers[31] enhanced the REE adsorption capacity. Further batch scale characterization with leachates prepared from legacy gold mine tailings (CO) and Round Top Mountain ores (TX) revealed that cell surface functionalization with LBT enhanced the selectivity of *E. coli* for all non-REEs except Cu, enabling high efficiency REE extraction from feedstock leachates.[27] However, the current form of most biosorbents, including LBT-displayed *E. coli*, restricts the biosorption process to batch scale operations that require energy and time intensive procedures such as centrifugation and/or filtration to separate the biomass from the feedstock,[32] limiting their industrial applicability.

To apply microbial biomass for efficient and scalable rare earth recovery, it is critical to immobilize cells at a high-density without compromising their adsorptive characteristics. Encapsulating microbes within a porous polymer matrix provides an effective means to stably immobilize cells and enable facile separation from aqueous solutions under flow. Several natural and synthetic polymers such as polyacrylamide,[33] polyethylene glycol,[34] cellulose,[35] polyvinyl alcohol,[36] silica,[37-39] and more commonly alginate,[36, 40-42] have been employed as support materials for cell immobilization. However, most applications with encapsulated microbes have focused on environmental remediation rather than the extraction and purification of critical metals for industrial purposes, where the purity of the recovered metals is critical.

Herein, we report several key advances toward implementing a biosorption-based flow-through process for selective recovery of critical metals from electronic wastes. A novel biosorbent was developed by encapsulating a high density of engineered *E. coli* cells in non-adsorptive (polyethylene glycol diacrylate) PEGDA hydrogel spheres and the REE extraction performance of the resulting microbe bead adsorbent was characterized in packed bed columns with synthetic solutions and an E-waste leachate.

Materials and Methods

Bacterial strains and growth conditions. An *E. coli* strain harboring an *lpp-ompA*-dLBTx8 expression plasmid[27] was grown in LB media supplemented with 50 μg/mL ampicillin. Expression of *lpp-ompA*-dLBTx8 was induced at mid-exponential phase using 0.002% arabinose for 3 hr at 37°C. The *E. coli* cells were harvested, washed once in 10 mM MES (2-(*N*-morpholino)ethanesulfonic acid; pH 6.0), and resuspended in 10 mM MES at an optical density at 600 nm (OD_{600}) of 40 (~$1x10^{11}$ cells/ml). This cell suspension was used directly for microbe bead synthesis.

Microbe bead synthesis. A bulk emulsion method was used to encapsulate LBT-displayed cells within PEGDA hydrogel spheres. The polymer precursor was prepared using 1% w/w TPO-L photoiniator (2,4,6-Trimethylbenzoylphenyl phosphinic acid ethyl ester; Rahn AG) and 99% w/w polyethylene glycol diacrylate (M_n 575; Sigma Aldrich). The polymer precursor was then mixed at 25% v/v with a concentrated cell suspension (75% v/v) containing ~$1x10^{11}$ cells/ml. The resulting aqueous phase was mixed 12.5% v/v in 40 mL silanized borosilicate vials with an oil phase, containing 1% w/w Triton X-100 surfactant (Sigma Aldrich) and 99 % w/w polydimethylsiloxane oil (10cSt PDMS oil; Clearco Products). The vials were agitated by external force for ~15 s to produce an emulsion and were immediately exposed to UV (4 W/cm^2 at 365 nm) for 120 s to polymerize the droplets comprised of PEGDA and LBT-displayed cells. The PDMS oil was removed from the polymerized microbe beads by vacuum filtration through a 20 μm nylon mesh filter and the microbe beads were rinsed 5-10 times in 0.9% w/v NaCl solution to remove any residual oil before storing in 10 mM piperazine-N,N′-bis(2-ethanesulfonic acid) (PIPES; pH 7) at ~4°C until use. No change in Nd adsorption capacity was observed after a storage period of 1 month at these conditions (Figure S1). We note that REE biosorption is not dependent on cell viability so neither the microbe synthesis or storage steps were conducted with the goal of preserving cell viability.

Prior to use, microbe beads were collected on a 20 μm nylon mesh filter, residual liquid was removed, and the wet weights of bead aliquots were measured. Dry weights (dw) of microbe beads were determined after heating the microbe bead aliquots at ~65°C for 72 hr. The fraction of the wet microbe bead mass contributed by water was determined by comparing the wet and dry weights and was found to be 76 ± 2.1 wt%. Minimal cell loss was observed after overnight shaking, based on OD_{600} measurements of the decanted supernatant, demonstrating the structural integrity of the microbe beads (data not shown). Based on the known cell and PEGDA masses added during bead synthesis, the dry microbe beads were calculated to be ~13 wt% cells and ~87 wt% PEGDA.

Batch sorption experiments. The microbe beads were distributed by wet weight into 5 mL Eppendorf tubes for batch adsorption experiments. 50 mM neodymium (Nd) and Gadolinium (Gd) stock solutions were prepared by dissolving $NdCl_3 \bullet 6H_2O$ or $GdCl_3 \bullet 6H_2O$ (Sigma Aldrich; 99.9% and 99% purity, respectively) in 1 mM HCl. Stock solutions were diluted in MES (10 mM, pH 6) for all assays. Thermodynamic analyses support high Nd solubility in pH 6 aqueous solutions.[43] For the batch adsorption capacity determination, 0.05 g (wet weight) of microbe beads was exposed to 0-300 μM Nd in 5 mL total volume. For the batch adsorption kinetics experiment, 5 mL of 500 μM Nd was added to 0.2 g (wet weight) of microbe beads. The tubes were mixed in a rotator for the duration of the experiments (60 minutes for the adsorption capacity test and 1-60 minutes for the adsorption kinetics test). Adsorbed Nd was calculated colorimetrically by determining the Nd concentration before and after the adsorption step using Arsenazo III (supporting information).

Breakthrough columns. Econo-Column glass chromatography columns (Bio-Rad) were packed with microbe beads or cell-free beads for continuous flow REE recovery experiments. A suspension of microbe beads was initially added to the columns (15 x 0.5 cm, 20 x 0.5 cm, and 100 x 1 cm) gravimetrically and then packed down by adding slight fluid pressure to the top of the column with a hand-operated syringe. Under pressure, the sorbent bed compressed and more microbe beads were added. This procedure was repeated until the entire column volume was filled. The microbe bead sorbent was conditioned with MES (10 mM, pH 6) at >5 times the bed volume in preparation for adsorption. The REE feedstock was then pumped through the column at a measured rate of 1 mL/min unless otherwise specified. For most tests, the feedstock Nd concentration was 500 μM Nd in MES (10 mM, pH 6). Homopiperazine-1,4-bis(2-ethanesulfonic acid) (10 mM) was used to buffer feedstocks at pH 4 and 5. The column effluent was collected in 1 mL aliquots and analyzed using Arsenazo III assays and/or Inductively coupled plasma mass spectrometry (Supporting Information). For column reuse experiments, Nd was desorbed with at least 10 bed volumes of sodium citrate (10 mM, pH 6) and then the columns were conditioned with MES (10 mM, pH 6) prior to reuse. Dry adsorbent weights were determined by removing the microbe beads from the columns and drying at ~65°C for 72 hours. The REE adsorption capacities of the fixed bed columns were calculated from the measured breakthrough curves via mass balance,[44] as follows:

$$q = \frac{QC_0 \int_{t=0}^{t=\infty} 1 - \frac{C}{C_0} dt - \varepsilon \frac{\pi D^2 L}{4} C_0}{m}$$

where q is the adsorption capacity (mg/g), Q is the feed flow rate (mL/min), C_0 is the feedstock Nd concentration (mg/mL), C is the effluent concentration (mg/mL), D is the column diameter (cm), L is the bed height (cm), ε is the bed void fraction (cm^3 void/cm^3 bed), m is the adsorbent mass, and t is time (min). The integral portion of the equation was numerically solved using the MATLAB trapezoidal numerical integration function (trapZ; R2017a). The void fraction (ε) of the packed column (~23% of the total column volume) was determined by analyzing the REE breakthrough behavior in a column packed with PEGDA beads without cells. Because PEGDA alone is not adsorptive, any delay in REE breakthrough in the no-cell column is due to the passage of void volume and dilution of the influent. An estimate of the void volume is calculated based on the extent of the observed delay. Breakthrough column modeling is described in the supporting information.

Leaching of NdFeB magnets. NdFeB magnet scraps and casings from speakers of mobile devices were separated from plastic and nonmetallic parts using hand held tools, demagnetized by heating in a muffle furnace at 400 °C for 1 h then incubated at a density of 1.5% (w/v) in H_2SO_4 (0.2 N) for two weeks at 20 °C. The pH of the resulting leachate (~pH of 3.7) was adjusted to 6 using NaOH and insoluble precipitates were removed through centrifugation at 20,000 *xg* and passage through a 0.2 µm filter immediately prior to column assays. We do not anticipate the addition of Na ions to affect the selectivity of the biosorption process given prior results that found Na to be minimally competitive with REEs for the engineered *E. coli* surface sites.[45] The pH adjustment resulted in a 75% reduction in the iron concentration, but the REE concentrations were unaffected (Table S1). While Fe(III) is expected to precipitate as a hydroxide species at this pH and Fe(II) spontaneously oxidizes to Fe(III), the residual Fe content in the leachate after filtration could either reflect the slow oxidation of Fe(II) to Fe(III), which has been previously suggested to explain Fe solubility in NdFeB leachates in the pH 5-6 range,[46] or the formation of soluble Fe(III) sulfate or carbonate complexes. Boron concentrations was not quantified in this study.

Results

Microbe bead synthesis. To produce a microbe bead adsorbent, we employed a bulk emulsification technique with UV-crosslinking to encapsulate REE-adsorbing bacteria at high cell-density in PEGDA. PEGDA was selected as the carrier material given its low cost, mechanical and chemical stability, ease of crosslinking, and lack of metal adsorption.[47, 48] The encapsulated *E. coli* cells were previously engineered for cell surface display of lanthanide binding tags and their selective REE adsorption has been shown in batch with geothermal fluids and mine tailing

leachates.[27, 45] In order to determine the optimal microbe bead formulation, the cell density and PEGDA concentration were varied. As expected, REE adsorption scaled in proportion to cell density between ~1.5×10^{10} and ~9.6×10^{10} cells/mL (Figure S2A). With a cell density above ~4.3×10^{10} cells/mL, a higher PEGDA content (>15 vol%) was required to maintain the physical integrity of the microbe beads. Increasing the PEGDA content between 10 and 25 vol% had a minimal negative effect on REE sorption (Figure S2B). Accordingly, all subsequent tests of microbe beads were formulated with ~10^{11} cells/mL in 25 vol% PEGDA.

Adsorption and desorption in batch reactions. The adsorption capacity of the microbe beads was determined in batch using equilibrium adsorption experiments in a synthetic solution (pH 6) containing Nd, a REE of high criticality that is abundant in many REE-bearing electronic wastes (Figure 1A). The adsorption data were fit with a Langmuir isotherm model (r^2 of 0.997), which revealed a maximum Nd adsorption capacity of ~2.64 mg Nd/g microbe bead dw. The adsorption capacity of control PEGDA beads lacking bacteria was negligible (Figure 1A), confirming that the encapsulated microbes were solely responsible for Nd adsorption. The reduced adsorption capacity of the microbe beads compared to cells alone (~25.7 mg Nd/g dry cells[27]) is expected given that PEGDA constitutes ~87% of the dry weight and is non-adsorptive. Overall, these data confirm that the cell surface sites of encapsulated cells are accessible for REE adsorption.

To further characterize the microbe bead function, Nd adsorption and desorption kinetics were assessed in batch reactions. Nd adsorption increased rapidly over the first 10 min, reaching ~90% of the calculated adsorption maximum (Figure 1B). To recover the adsorbed Nd, desorption was performed using sodium citrate (10 mM, pH 6), which was previously found to enable complete elution of adsorbed REEs.[27, 28] Faster kinetics was observed during desorption, with near complete Nd recovery achieved within 5 min (Figure 1C). To determine the extent to which cell encapsulation affects the adsorption/desorption kinetics, control experiments were performed with free cells using the same approximate biomass concentration and equivalent experimental conditions. Faster adsorption and desorption kinetics were observed compared to the microbe beads, with >80% of the Nd adsorption maximum and near complete Nd desorption achieved within 1 min (Figure 1B-C). From these data, we conclude that intraparticle diffusivity (IPD), i.e. the transport of Nd or citrate from the external surface into the PEGDA pores, is likely the dominant factor that controls Nd adsorption and desorption kinetics in the microbe beads. Nonetheless, the adsorption/desorption kinetics observed for the microbe beads is suitable for continuous flow applications.

Accordingly, the intraparticle diffusivity was determined by fitting the bead kinetics data using the Vermeulen model (i.e., pore-surface mass diffusion model), which describes the diffusion in a spherical adsorbent particle (Figure 1B-C). The model produced reasonable fits for both data sets (r^2 of 0.98 for both) and predicted an intraparticle diffusivity of 4.1 x 10^{-7} and 1.5 x 10^{-6} cm^2/min for adsorption and desorption, respectively. These diffusion values are qualitatively consistent with the experimentally determined intraparticle diffusion rates for other small molecules, such as a lithium tetra(ethylene glycol) dimethyl ether complex (6.06 x10^{-7} cm^2/min[49]), Texas Red (2.52 x10^{-7} cm^2/min[50]), and Tetramethylrhodamine isothiocyanate (8.40 x10^{-7} cm^2/min[51]), in comparable PEGDA polymers (PEGDA 575-1000). As such, we anticipate that intraparticle diffusion will impact the kinetics of REE adsorption in a continuous flow process involving microbe beads.

Microbe bead morphology and cell distribution. The microbe bead morphology, size range, and cell distribution were determined using several complementary microscopy techniques. Scanning helium ion microscopy (HIM) analysis revealed that the microbe beads were spherical or a cluster of multiple spherical particles and exhibited an average diameter of 59 ± 24 μm (n=72) (Figure 2A; Figure S3). In some instances, beads were connected through small protrusions (Figure S4). The microbe beads exhibited a rough outer surface morphology as a consequence of partially encapsulated cells at the exterior (Figure 2B-C) and this morphology was not altered following a single adsorption/desorption cycle with citrate (Figure S5). The lack of visible pore structures within the microbe beads is consistent with a reported mesh size for similar composition PEGDA hydrogels (M_n 575-20000) of ~1-2 nm,[51-53] which approaches the resolution limit for HIM. Given aqueous ionic radii for lanthanides of ~0.25 nm[54] and a hydrodynamic radius of 0.37 nm for the eluent citrate,[55] we anticipate that this pore structure is sufficiently permeable for both the REE biosorption and desorption steps. Both confocal microscopy and TEM with thin-sectioned microbe beads suggested that the cells were homogenously distributed within the microbe beads (Figure 2D-E). Unsurprisingly, some instances of cell lysis and aggregated cell debris were observed within the sectioned microbe beads (Figure S6). Given the small pore size, we expect this aggregated material to be contained within the microbe bead and to contribute to REE biosorption.

To confirm REE penetration and adsorption within microbe beads, MRI was performed on microbe beads with or without Gd exposure. Based on its paramagnetic properties, Gd shortens transverse relaxation times (T_2) in materials where it has accumulated. T_2-weighted images revealed lower relaxation times (i.e., brighter images) for

microbe beads with adsorbed Gd (Figure 2G) compared to microbe beads without Gd exposure (Figure 2I) or after Gd was desorbed using citrate (Figure 2H), an effective eluent previously used to recover REEs from LBT-displayed cells.[27, 28] The fluctuations in image intensity in the negative control images (Figure 2H-I) may be attributed to differences in spin density (i.e., the concentration of protons). The cell-specific association of REEs within microbe beads was further demonstrated using thin section TEM coupled with energy-dispersive X-ray spectroscopy (Figure S7) and the data are discussed in the supporting text. Collectively, these imaging results support the stable encapsulation and cell surface accessibility of a dense population of *E. coli* cells within a PEGDA matrix.

REE adsorption in a fixed-bed column. To test the efficacy of the microbe beads for REE extraction under continuous flow, fixed-bed columns were packed with the microbe bead adsorbent and influent breakthrough behavior was assessed with synthetic solutions containing Nd. The Nd breakthrough point (operationally defined as C/C_0 of 0.05) with the microbe beads occurred after ~7 bed volumes, in contrast to 0.5 bed volumes with the cell-free beads, which is due only to the passage of the void volume rather than adsorption (Figure 3). The adsorption capacity of the microbe bead column (~2.6 mg/dry g; Table S2), determined by mass balance, was nearly equivalent to that determined in the batch adsorption experiment (Figure 1A), indicating that microbial surface accessibility was not limited by these initial flow parameters (3 m/h linear flow velocity).

The observed Nd breakthrough curve with the microbe bead adsorbent was asymmetrical; the leading-edge feature (i.e., the breakthrough feature) occurred over a narrow volume range while the trailing edge feature (i.e., approach of C/C_0 towards 1) was more gradual. This tailing effect is commonly observed in packed bed columns when intraparticle diffusion is the dominant mass transfer process,[56] consistent with the batch kinetics results (Figure 1B). As such, the Bohart-Adams model, a commonly employed fixed bed model that does not account for IPD and produces a centrosymmetric curve fit, did not accurately model the asymmetric trailing and leading-edge features of the breakthrough curve. However, a modified Bohart-Adams model,[57] which yields an asymmetric breakthrough curve through the introduction of a fractal-like exponent, provided an improved empirical fit to the breakthrough data (Figure 3; Table S2) and was used to model the Nd data in subsequent experiments. The improved fit of the fractal-like Bohart-Adams model is consistent with the results for several distinct porous adsorbents.[57] Future work will include the development of a theoretical model that incorporates mass transfer

effects, such as the advective transport through the column coupled with diffusive and dispersive transport within the intra-bead region.

Effect of system variables on REE adsorption in a fixed-bed column. A series of breakthrough curves was performed to determine the effects of linear flow velocity, REE concentration, and pH on column dynamics. The Nd breakthrough point was inversely proportional to the influent Nd concentration (Figure 4A-B). As expected, there was a slight increase in the bed adsorption capacity with increasing influent Nd concentration, with a capacity of 2.8 mg/g microbe bead dw at 1.5 mM Nd compared to 2.3 mg/g microbe bead dw at 50 μM Nd (Table S3). Linear flow velocities of 1.5 and 3 m/h yielded nearly identical breakthrough points and bed capacities (Figure 4B, Table S3). However, increasing the flow velocity above 3 m/h caused increasingly early Nd breakthrough and significantly reduced the bed capacity, with 1.9 and 1.8 mg/g microbe bead dw observed at flow velocities of 6 m/h and 15 m/h, respectively, compared to 2.6 mg/g microbe bead dw at 3 m/h. A decrease in column adsorption capacity with increasing flow rate is commonly observed in fixed-bed column studies and has been attributed to a failure to reach equilibrium.[44, 58, 59] Alternatively, it is possible that high flow rates cause a fraction of the available binding sites to be physically blocked, perhaps due to bead deformation caused by increased pressure in the column. Based on these results, we conclude that the current version of microbe beads enable robust REE extraction at Nd concentrations up to 1.5 mM and linear flow velocities up to 3 m/h.

To examine the effect of influent pH on column performance, breakthrough curves were performed over a pH range of 4-6 (Figure 4C). This pH range was selected based on the lower expected REE solubility above pH 6 and prior characterization of LBT-displayed *E. coli*, which revealed a significant reduction in REE adsorption capacity at a pH below 4.[45] Consistent with the prior batch studies with LBT-displayed cells,[28, 45] the breakthrough points and bed adsorption capacities were proportional to the influent pH. Bed capacity was reduced from 2.6 at pH 6 to 1.8 and 1.1 mg/g microbe bead dw at pH 5 and 4, respectively (Figure 4C, Table S2). These data suggest that while optimal REE extraction performance is achieved at pH 6, the microbe beads are likely amenable, albeit with reduced performance, to REE extraction with feedstocks in which limited REE solubility requires a lower system pH.

Microbe bead column reusability. Column reusability is a critical factor for economic feasibility and therefore the extent to which a microbe bead column can sustain multiple rounds of adsorption/desorption was examined. As a

first step, we tested the efficacy of citrate to elute adsorbed REEs from the column following a 5x bed volume wash step (MES pH 6) to clear non-adsorbed Nd from pore spaces. High efficiency (~94%) Nd desorption was achieved with a 10 mM citrate solution (pH 6) within 3 bed volumes (Figure 5A), confirming the utility of citrate as an effective eluent in a column setting. This result also demonstrated the concentrating effect of the citrate desorption step, with the Nd concentration increased by as much as 6-fold for some fractions. A higher concentrating factor may be achieved by re-circulating a small volume of citrate. To assess column reusability, nine consecutive adsorption/desorption cycles were run on the same column (Figure 5B) with each cycle consisting of an adsorption step with 500 μM Nd (pH 6) and a desorption step with 10 mM citrate (pH 6). A small, gradual decrease in bed capacity (~15% overall) was observed over the course of the first five cycles, reflected in progressively earlier Nd breakthrough points (Figure 5B). The bed capacity and breakthrough points appeared to stabilize after five cycles (Figure 5C). We attribute this gradual performance loss to either reduced column porosity caused by irreversible bead deformation over time or loss of incompletely encapsulated cells, such as those located at the periphery of the microbe beads (Figure 2C). Nevertheless, the limited reduction in Nd extraction performance over the course of nine adsorption/desorption cycles is indicative of promising microbe bead reusability.

REE extraction from an electronic waste leachate. To test the efficacy of microbe beads to extract REEs from an end-of-life feedstock, NdFeB magnet scraps from speakers of mobile devices were leached with sulfuric acid and the pH was adjusted to 6. The pH-adjusted leachate contained 700 μM total REEs (Nd, Pr, Dy) and a total of ~1.5 mM of the transition metals Fe, Zn, Ni, Mn, and Co (Table S4). Initial, small-scale (1.5 mL) batch biosorption assays performed with free LBT-displayed *E. coli* over a range of biomass concentrations revealed that REEs could be extracted from the NdFeB magnet leachate with high efficiency and purity; at the optimal cell density, 91% of the REEs were extracted at a purity of 95% (Figure 6A). To test the feasibility of bench scale REE extraction under flow through conditions, we performed a breakthrough experiment using a 1 x 100 cm (77 mL) microbe bead column. The effluent metal concentrations were quantified over four bed volumes and the time-course adsorption profile for each metal ion was calculated using mass balance (Figure 6B-C; Figure S8). Consistent with the high REE selectivity observed for LBT-*E. coli* in batch (Figure 6A), non-REE metal adsorption was minimal with transition metal breakthrough observed within a single bed volume (Figure 6B). The non-REE metals, Fe, Ni, Mn, Co, and Zn broke through at approximately the same point; however, the Fe, Ni, Mn, and Co

effluent concentrations exceeded the influent concentrations following breakthrough ($C/C_0 > 1$). In contrast, the saturation point of Zn was reached without this overshoot ($C/C_0 \approx 1$). This behavior is likely indicative of competitive displacement (i.e., ion exchange) of Fe, Ni, Mn, and Co by Zn and the REEs, which causes the effluent concentrations to reflect the sum of the influent and desorbed ion concentrations. Breakthrough of the REEs Pr, Nd, and Dy occurred after ~3 bed volumes and coincided with a pronounced overshoot of Zn, reflecting competitive displacement of Zn. At the REE breakthrough point, REEs comprised 97% of the adsorbed metals by mass, with only a minimal increase in purity expected beyond the breakthrough point (Figure 6D).

Although breakthrough of Pr, Nd, and Dy (Figure 6B) occurred over a narrow volume range, there were notable differences in the breakthrough curve slopes. In comparison to Nd and Pr, Dy exhibited a more gently sloped breakthrough curve that is indicative of its higher binding affinity and ability to compete for sites pre-occupied by the other REEs present. The higher affinity of the microbe beads for Dy is consistent with the general preference of LBT-displayed cells for REEs of smaller atomic radii.[27] Collectively, these data support the efficacy of the microbe beads to selectively extract REEs from a post-consumer E-waste feedstock leachate and confirm that PEGDA encapsulation does not adversely affect the selectivity of LBT-*E. coli* cells .

Discussion

This study was undertaken to develop a cell immobilization system to enable a scalable, flow-through biosorption-based operation for REE recovery from feedstock leachates. While the REE adsorption properties and mechanisms of numerous biosorbents have been reported,[19, 22, 60] very few have been developed for a flow-through operation,[31, 33] or validated with real world REE feedstocks.[27, 35, 61] As a step toward addressing these limitations, which hinder the scalability of the biosorption process, we demonstrated a PEGDA emulsion method to stably encapsulate bacterial cells as small spherical microbe beads (~60 μm diameter). This emulsion process could be applied at an industrial scale through the use of continuous-flow UV polymerization combined with an in-line mixer.[62] In further support of scalability, we demonstrated the use of microbe bead resin for flow-through REE extraction with an electronic waste leachate in a packed-bed column format (77 ml total volume) that is commonly employed for adsorption in chemical process industries. As such, this study lays the groundwork for the development of biosorption for industrial-scale REE/metal recovery.

The use of a non-adsorptive support matrix (i.e., PEGDA) allows the selectivity of the encapsulate (i.e., LBT-*E. coli)* to dictate the purity of the extracted solution and avoids the potential for matrix-mediated sorption of contaminant metals. However, the superior selectivity of the PEGDA-based encapsulation approach comes at a cost of adsorption capacity; the current microbe bead adsorption capacity (2.6 mg/g) is relatively low on a per mass basis compared to unencapsulated microorganisms[19, 60] or ligand-functionalized solid phase adsorbents (0.83-176 mg/g).[63] A recent report described a cellulose encapsulated yeast biosorbent for Eu recovery from phosphor powder leachates with an adsorption capacity of 25.9 mg/g.[35] However, the effect of the cellulose support matrix, which dominated Eu sorption, was not characterized.[35] A further improvement in adsorption capacity will be required to make the microbe bead biosorbent more attractive at an industrial scale, and could be achieved by increasing the cell:polymer ratio, genetic engineering to increase the number of cell surface functional groups per unit mass, and/or screening for microbes with higher metal adsorption capacity.

The application of the microbe bead biosorption technology for REE extraction from feedstocks would require post-biosorption steps to produce a salable product. Based on the breakthrough column results, a concentrated REE citrate solution can be generated using a circulating citrate desorption step. Subsequently, the mixed REE-citrate solution would be subjected to precipitation (e.g., as hydroxides, oxalates, or double sulfate salts)[64] and roasting to produce high-purity mixed Nd-Pr-Dy oxides, which would approximate the composition of the dissolved magnet scrap feedstock. As such, it is perceivable that this Nd-Pr-Dy oxide blend, perhaps with a minor adjustment in composition, could be directly used in magnet manufacturing without the need for purification of individual REEs. For this reason, several recent reports on REE recovery from NdFeB magnets have targeted a mixed Nd-Pr-Dy final product.[46, 65, 66] We have previously examined the technoeconomic feasibility for applying biosorption in a large-scale process for the production of mixed REE oxides from a range of primary feedstocks.[67] While favorable economics were obtained for feedstocks that contain high value REEs (e.g., scandium), the low revenue from producing low-value mixed REOs makes individual, separated REEs a more desirable end product. REE separation would also be beneficial for feedstocks of mixed E-wastes that contain magnets of different compositions. A prior study by Bonificio and Clarke (2016) supports the feasibility of biosorption-based REE separation using bacterial surfaces, reporting separation factors among REE pairs that rival that of solvent

extraction.[29] Future efforts for REE separation will seek to incorporate a differential desorption step to further exploit the selectivity differences among REEs observed for the adsorption step.

In conclusion, we have developed a generalizable biomass immobilization platform for the selective grouped extraction of trivalent REEs from complex mixtures of metals. We focused on REE extraction from magnet scraps since this application has the potential to contribute to the circular REE economy and reduce the dependence on REE mining. However, we anticipate that the microbe beads will have similar utility for alternative REE feedstock leachates such as ores, mine tailings, and coal byproducts, based on the selective adsorption of REEs from these feedstocks using unencapsulated LBT-displayed *E. coli* in batch.[27] More broadly, this technology may have application in areas beyond REE recovery, such as trivalent metal separation from d-block impurities during spent nuclear fuel reprocessing.

Supporting Information

Supplemental methods; supplemental text; Table S1, Metal ion composition of E-waste leachate before and after pH adjustment; Table S2, Effect of pH on microbe bead Nd adsorption in a fixed-bed column; Table S3, Effect of linear flow velocity and Nd concentration on fixed bed column performance; Table S4, Metal composition of E-waste leachate; Figure S1, Stability of the microbe beads during storage; Figure S2, Effect of cell density and polymer fraction on microbe bead adsorption performance; Figure S3, Microbe bead size distribution; Figure S4, HIM images depicting representative examples of bead fusions and protrusions; Figure S5, HIM images depicting representative examples of microbe beads before and after treatment with 10 mM citrate; Figure S6, Thin section TEM images depicting some instances of cell lysis and aggregated cell debris within the PEGDA polymer at different magnifications; Figure S7, Cell-association of Nd within microbe beads; Figure S8, E-waste breakthrough curve presented with the absolute metal concentrations in the effluent; Figure S9, Mineral precipitates were not observed in microbe beads lacking Nd; Figure S10, Colorimetric and ICP-MS quantification of Nd concentrations for a representative breakthrough curve;

Acknowledgements

We thank Kevin Paulsen for his assistance silanizing the borosilicate vials, Mathew Yim for assistance in magnet disassembly and leaching, and Gauthier Deblonde for helpful comments on the manuscript. AB acknowledges funding from the Livermore Graduate Scholar Program from Lawrence Livermore National Laboratory. HIM and TEM were performed in EMSL, a DOE Office of Science User Facility sponsored by the Office of Biological and Environmental Research and located at Pacific Northwest National Laboratory. This research is supported by the Critical Materials Institute, an Energy Innovation Hub funded by the U.S. Department of Energy, Office of Energy Efficiency and Renewable Energy, Advanced Manufacturing Office, and by the Department of Energy through the Technology Commercialization Fund (TCF). This work was performed under the auspices of the U.S. Department of Energy by Lawrence Livermore National Laboratory under Contract DEAC52-07NA27344 (LLNL-JRNL-767490) and by Idaho National Laboratory under DOE Idaho Operations Office Contract DE-AC07-05ID14517.

Conflict of interest statement

LBT-displayed *E. coli* is included in a prior patent (US 10,196,708) and portions of this study are included in a pending patent (16/289,382).

Figures

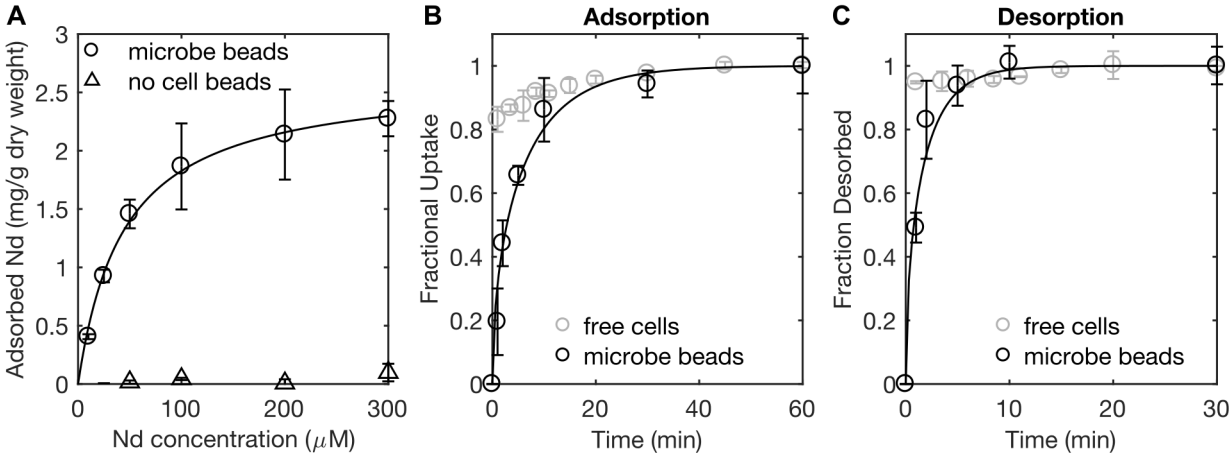

Figure 1: Nd adsorption isotherm and kinetics by microbe beads and free cells. (A) Nd adsorption isotherm with microbe beads (circles) and beads without cells (triangles). Experimental data were fit to a Langmuir isotherm (solid line) using nonlinear regression. (B) Nd adsorption kinetics of microbe beads (black circles) in comparison to free cells (gray circles). MES solution (10 mM, pH 6) containing 500 μM Nd was used. (C) Nd desorption kinetics using citrate solution (10 mM, pH 6) with microbe beads (black circles) in comparison to free cells (gray circles). The kinetics data were fit with the Vermeulen model (black line) and yielded correlation coefficient r^2 values of 0.98 for both adsorption and desorption.

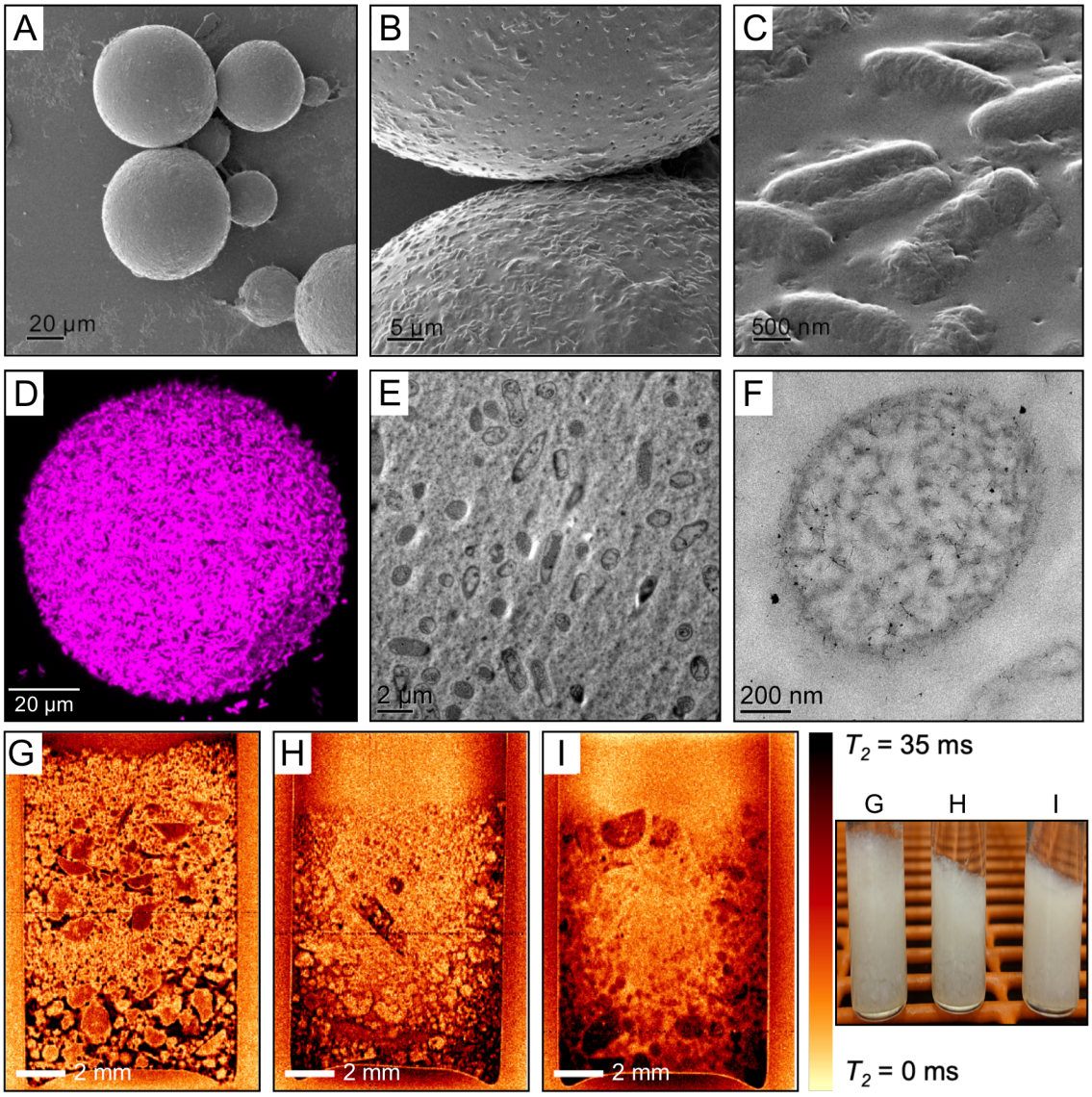

Figure 2. Microbe bead imaging. (A-C) Helium ion microscopy images of microbe beads at different magnification. At high magnification, encapsulated *E. coli* are visible on the microbe bead surface. **(D)** Confocal microscope image showing a 3-D reconstruction of a representative microbe bead from Z stack images. Cells were visualized by staining with propidium iodide. The image depicts the dense and homogeneous distribution of cells across the surface of the microbe beads and confirms their mortality. **(E)** TEM image of a microbe bead cross-section showing individual cells imbedded in the PEDGA polymer. **(F)** TEM image of a representative cell from a Nd-adsorbed microbe bead showing cell-associated needle-like biogenic minerals (See supporting information for more details). T_2-weighted MRI of microbe beads packed in 1 cm outer diameter NMR tubes with adsorbed Gd **(G)**, following citrate (10 mM, pH 6)-mediated desorption **(H)**, or without Gd exposure **(I)**. The hotiron- LUT was

used for all MRI images. A picture of the microbe bead-containing NMR tubes is depicted to the right of the MRI images as a reference.

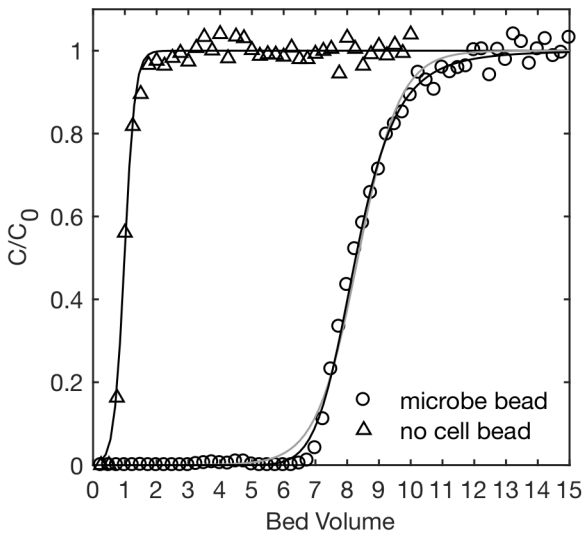

Figure 3: Nd adsorption in a fixed bed column with microbe beads. Columns (20 cm x 0.5 cm) were packed with microbe beads (circles) or beads without cells (triangles). Breakthrough curves were performed at a linear flow velocity of 3 m/h with an influent solution containing 500 µM Nd and MES (10 mM, pH 6). The data were fit to the classical Bohart-Adams kinetic model (gray line) and the fractal-like Bohart-Adams model (black line)[57] using non-linear regression. The parameters obtained from the Bohart-Adams models are displayed in Table S2.

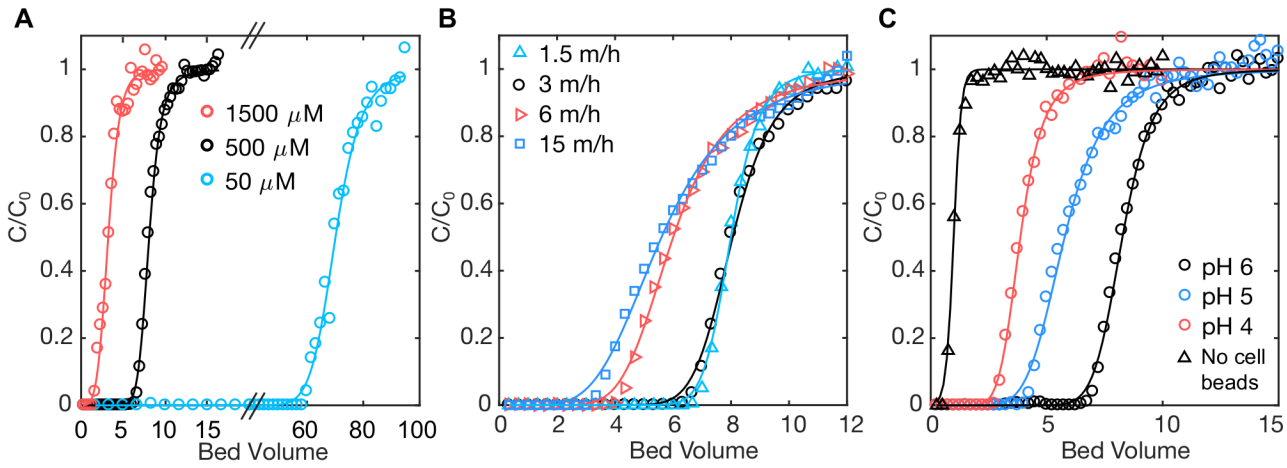

Figure 4: Breakthrough curves depicting the effect of system variables on column dynamics for columns packed with microbe beads. (A) Effect of influent REE concentration: influent solution of MES (10 mM, pH 6) containing 50, 500, or 1500 µM Nd at a linear flow velocity of 3 m/h. **(B)** Effect of linear flow velocity (m/h) on

Nd breakthrough behavior at a fixed Nd concentration of 500 µM. The linear flow velocity was defined as the volumetric flow rate (m^3/h) per unit cross-sectional area (m^2) of the column. **(C)** Effect of influent pH: influent of pH 4, 5, or 6 containing a fixed concentration of 500 µM Nd at a linear flow velocity of 3 m/h. The influent was buffered with HomoPIPES (10 mM, pH 4 or 5) or MES (10 mM, pH 6). The column dimensions were 15 cm x 0.5 cm for the breakthrough columns depicted in panels A-B and 20 cm x 0.5 cm for the data depicted in panel C. The data were fit to the fractal-like Bohart-Adams model (colored lines) and parameters obtained from the model are displayed in Table S2-S3.

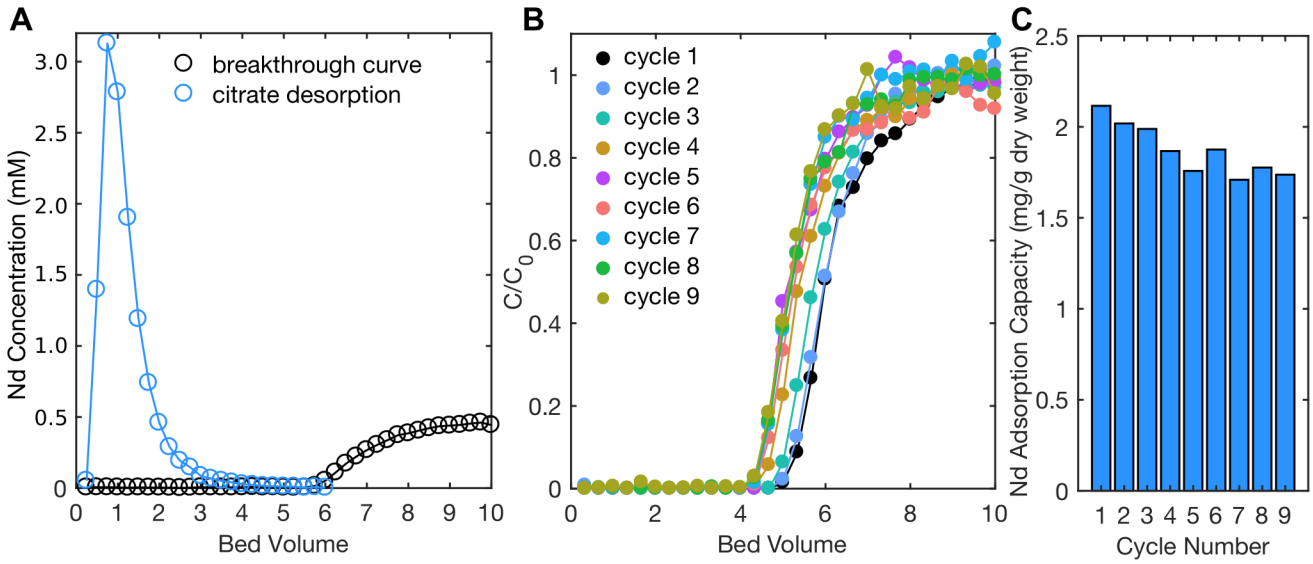

Figure 5: Column reusability tests. (A) Citrate elution profile for column (20 cm x 0.5 cm). The corresponding breakthrough curve for the adsorption step is plotted for reference. **(B)** Nd breakthrough curves for each of 9 consecutive adsorption/desorption cycles at a linear flow velocity of 3 m/h. For each cycle, an influent of 500 µM Nd in MES buffer (10 mM, pH 6) was used for adsorption and 35 ml of 10 mM citrate for desorption. The column (15 cm x 0.5 cm) was washed with 100 ml MES buffer between each adsorption/desorption cycle. **(C)** Bed adsorption capacity calculated for each consecutive adsorption cycle using mass balance.

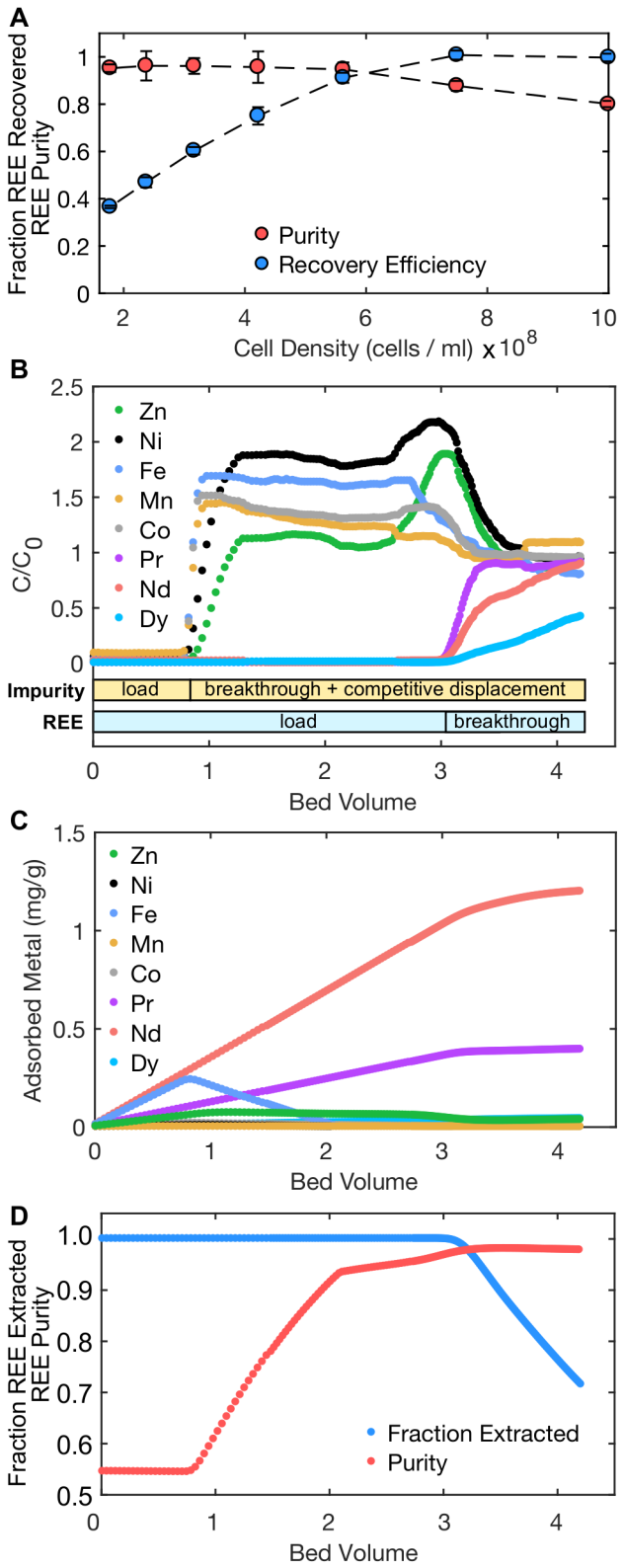

Figure 6: Bath and continuous flow REE extraction from an electronic waste leachate. (A) REE recovery efficiency and purity as a function of cell density for non-encapsulated LBT-displayed *E. coli*. Biosorption was performed in batch over a range of cell densities in the pH-adjusted E-waste leachate and the adsorbed metal ions

were desorbed using 5 mM citrate (pH 6). REE purity was defined as the weight percent REEs of the total metal content in the citrate eluent. The pH (6)-adjusted E-waste leachate described in Table S1 was diluted 20-fold prior to batch experiments, which were performed in duplicate. Error bars represent the standard deviation calculated using a formula for propagation of standard error.[68] **(B)** Breakthrough curve for metal ions in the E-waste leachate. E-waste leachates prepared with sulfuric acid were diluted 10-fold and adjusted to pH 6 prior to use as the influent in a column (~77 ml bed capacity, 100 cm x 1 cm) packed with microbe beads. The metal ion concentrations are described in Table S4. A linear flow velocity of 0.76 m/h was employed and 1 ml (0.01 bed volume) fractions were collected. Metal concentrations were quantified by ICP-MS and the data were median smoothed over a 10 ml (0.13 bed volume) window. The REE and non-REE (i.e., impurity) loading and breakthrough regions are summarized below the plot. A breakthrough curve depicting the absolute metal concentrations is presented in Figure S8. **(C)** The time-course adsorption profile for each metal ion was calculated using mass balance (see methods). **(D)** Fraction REE extracted and REE purity as a function of bed volumes. REE purity, defined in panel A, was determined using the mass balance data in panel C. The fraction of REE extracted was determined using the effluent Nd, Pr, and Dy concentrations.

References

[1] Alonso, E., Sherman, A. M., Wallington, T. J., Everson, M. P., Field, F. R., Roth, R., and Kirchain, R. E. (2012) Evaluating rare earth element availability: a case with revolutionary demand from clean technologies, *Environ Sci Technol 46*, 3406-3414.

[2] Weng, Z., Jowitt, S. M., Mudd, G. M., and Haque, N. (2015) A Detailed Assessment of Global Rare Earth Element Resources: Opportunities and Challenges*, *Economic Geology 110*, 1925-1952.

[3] Zhou, B. L., Z.;Chen, C. (2017) Global potential of rare earth resources and rare earth demand from clean technologies, *Minerals 7*, 1-14.

[4] Eggert, R., Wadia, C., Anderson, C., Bauer, D., Fields, F., Meinert, L., and Taylor, P. (2016) Rare Earths: Market Disruption, Innovation, and Global Supply Chains, *Annual Review of Environment and Resources 41*, 199-222.

[5] Massari, S., and Ruberti, M. (2013) Rare earth elements as critical raw materials: Focus on international markets and future strategies, *Resour Policy 38*, 36-43.

[6] Jha, M. K., Kumari, A., Panda, R., Rajesh Kumar, J., Yoo, K., and Lee, J. Y. (2016) Review on hydrometallurgical recovery of rare earth metals, *Hydrometallurgy 165, Part 1*, 2-26.

[7] Ali, S. (2014) Social and Environmental Impact of the Rare Earth Industries, *Resources 3*, 123-134.

[8] Law, Y.-H. (2019) Radioactive waste standoff could slash high tech's supply of rare earth elements, *Science*.

[9] Xie, F., Zhang, T. A., Dreisinger, D., and Doyle, F. (2014) A critical review on solvent extraction of rare earths from aqueous solutions, *Miner Eng 56*, 10-28.

[10] Haque, N., Hughes, A., Lim, S., and Vernon, C. (2014) Rare Earth Elements: Overview of Mining, Mineralogy, Uses, Sustainability and Environmental Impact, *Resources 3*, 614-635.

[11] Jowitt, S. M., Werner, T. T., Weng, Z., and Mudd, G. M. (2018) Recycling of the rare earth elements, *Current Opinion in Green and Sustainable Chemistry 13*, 1-7.

[12] Yang, Y., Walton, A., Sheridan, R., Güth, K., Gauß, R., Gutfleisch, O., Buchert, M., Steenari, B.-M., Van Gerven, T., Jones, P. T., and Binnemans, K. (2017) REE Recovery from End-of-Life NdFeB Permanent Magnet Scrap: A Critical Review, *Journal of Sustainable Metallurgy 3*, 122-149.

[13] Binnemans, K., Jones, P. T., Blanpain, B., Van Gerven, T., Yang, Y., Walton, A., and Buchert, M. (2013) Recycling of rare earths: a critical review, *Journal of Cleaner Production 51*, 1-22.

[14] Tunsu, C. (2018) 8 - Hydrometallurgy in the recycling of spent NdFeB permanent magnets, In *Waste Electrical and Electronic Equipment Recycling* (Vegliò, F., and Birloaga, I., Eds.), pp 175-211, Woodhead Publishing.

[15] DOE. (2011) Critical Materials Strategy.

[16] Hu, Y. M., Florek, J., Lariviere, D., Fontaine, F. G., and Kleitz, F. (2018) Recent Advances in the Separation of Rare Earth Elements Using Mesoporous Hybrid Materials, *Chem Rec 18*, 1261-1276.

[17] Murty, D. S. R., and Chakrapani, G. (1996) Preconcentration of rare earth elements on activated carbon and its application to groundwater and sea-water analysis, *Journal of Analytical Atomic Spectrometry 11*, 815-820.

[18] Awwad, N. S., Gad, H. M. H., Ahmad, M. I., and Aly, H. F. (2010) Sorption of lanthanum and erbium from aqueous solution by activated carbon prepared from rice husk, *Colloids and Surfaces B: Biointerfaces 81*, 593-599.

[19] Anastopoulos, I., Bhatnagar, A., and Lima, E. C. (2016) Adsorption of rare earth metals: A review of recent literature, *Journal of Molecular Liquids 221*, 954-962.

[20] Hadjittofi, L., Charalambous, S., and Pashalidis, I. (2016) Removal of trivalent samarium from aqueous solutions by activated biochar derived from cactus fibres, *Journal of Rare Earths 34*, 99-104.

[21] Gupta, N. K., Gupta, A., Ramteke, P., Sahoo, H., and Sengupta, A. (2019) Biosorption-a green method for the preconcentration of rare earth elements (REEs) from waste solutions: A review, *Journal of Molecular Liquids 274*, 148-164.

[22] Moriwaki, H., and Yamamoto, H. (2013) Interactions of microorganisms with rare earth ions and their utilization for separation and environmental technology, *Appl Microbiol Biotechnol 97*, 1-8.

[23] Texier, A.-C., Andrès, Y., and Le Cloirec, P. (1999) Selective Biosorption of Lanthanide (La, Eu, Yb) Ions by *Pseudomonas aeruginosa*, *Environ Sci Technol 33*, 489-495.

[24] Fein, J. B., Martin, A. M., and Wightman, P. G. (2001) Metal adsorption onto bacterial surfaces: development of a predictive approach, *Geochim Cosmochim Ac 65*, 4267-4273.

[25] Tsuruta, T. (2006) Selective accumulation of light or heavy rare earth elements using gram-positive bacteria, *Colloid and Surface B 52*, 117-122.

[26] Moriwaki, H., Koide, R., Yoshikawa, R., Warabino, Y., and Yamamoto, H. (2013) Adsorption of rare earth ions onto the cell walls of wild-type and lipoteichoic acid-defective strains of *Bacillus subtilis*, *Appl Microbiol Biotechnol 97*, 3721-3728.

[27] Park, D. M., Brewer, A., Reed, D. W., Lammers, L. N., and Jiao, Y. (2017) Recovery of Rare Earth Elements from Low-Grade Feedstock Leachates Using Engineered Bacteria, *Environ Sci Technol 51*, 13471-13480.

[28] Park, D. M., Reed, D. W., Yung, M. C., Eslamimanesh, A., Lencka, M. M., Anderko, A., Fujita, Y., Riman, R. E., Navrotsky, A., and Jiao, Y. (2016) Bioadsorption of Rare Earth Elements through Cell Surface Display of Lanthanide Binding Tags, *Environ Sci Technol 50*, 2735-2742.

[29] Bonificio, W. D., and Clarke, D. R. (2016) Rare-Earth Separation Using Bacteria, *Environ Sci Tech Let 3*, 180-184.

[30] Moriwaki, H., Masuda, R., Yamazaki, Y., Horiuchi, K., Miyashita, M., Kasahara, J., Tanaka, T., and Yamamoto, H. (2016) Application of Freeze-Dried Powders of Genetically Engineered Microbial Strains as Adsorbents for Rare Earth Metal Ions, *ACS Applied Materials & Interfaces 8*, 26524-26531.

[31] Tay, P. K. R., Manjula-Basavanna, A., and Joshi, N. S. (2018) Repurposing bacterial extracellular matrix for selective and differential abstraction of rare earth elements, *Green Chemistry 20*, 3512-3520.

[32] Dodson, J. R., Parker, H. L., Muñoz García, A., Hicken, A., Asemave, K., Farmer, T. J., He, H., Clark, J. H., and Hunt, A. J. (2015) Bio-derived materials as a green route for precious & critical metal recovery and re-use, *Green Chemistry 17*, 1951-1965.

[33] Texier, A. C., Andres, Y., Faur-Brasquet, C., and Le Cloirec, P. (2002) Fixed-bed study for lanthanide (La, Eu, Yb) ions removal from aqueous solutions by immobilized Pseudomonas aeruginosa: experimental data and modelization, *Chemosphere 47*, 333-342.

[34] Lee, K. G., Park, T. J., Soo, S. Y., Wang, K. W., Kim, B. I., Park, J. H., Lee, C. S., Kim, D. H., and Lee, S. J. (2010) Synthesis and utilization of E. coli-encapsulated PEG-based microdroplet using a microfluidic chip for biological application, *Biotechnol Bioeng 107*, 747-751.

[35] Arunraj, B., Sathvika, T., Rajesh, V., and Rajesh, N. (2019) Cellulose and Saccharomyces cerevisiae Embark To Recover Europium from Phosphor Powder, *ACS Omega 4*, 940-952.

[36] Tsekova, K. T., D.; Ganeva, S. (2010) Removal of heavy metals from industrial wastewater by free and immobilized cells of Aspergillus niger, *International Biodeterioration & Biodegradation 64*, 447-451.

[37] Cabuk, A., Akar, T., Tunali, S., and Tabak, O. (2006) Biosorption characteristics of *Bacillus* sp ATS-2 immobilized in silica gel for removal of Pb(II), *Journal of Hazardous Materials 136*, 317-323.

[38] Benson, J. J., Wackett, L. P., and Aksan, A. (2016) Production of monodisperse silica gel microspheres for bioencapsulation by extrusion into an oil cross-flow, *J Microencapsul 33*, 412-420.

[39] Mutlu, B. R., Yeom, S., Tong, H.-W., Wackett, L. P., and Aksan, A. (2013) Silicon alkoxide cross-linked silica nanoparticle gels for encapsulation of bacterial biocatalysts, *Journal of Materials Chemistry A 1*, 11051-11060.

[40] Xu, J., Song, X. C., Zhang, Q., Pan, H., Liang, Y., Fan, X. W., and Li, Y. Z. (2011) Characterization of metal removal of immobilized Bacillus strain CR-7 biomass from aqueous solutions, *J Hazard Mater 187*, 450-458.

[41] Preetha, B. V., T. (2007) Batch and continuous biosorption of chromium(VI) by Rhizopus arrhizus, *Separation and Purification Technology 57*, 126-133.

[42] Kuhn, S. P. P., R.M. (1989) Adsorption of mixed metals and cadmium by calcium-alginate immobilized Zoogloea ramigera, *Appl Microbiol Biot 31*, 613-618.
[43] Neck, V., Altmaier, M., Rabung, T., Lützenkirchen, J., and Fanghaenel, T. (2009) Thermodynamics of trivalent actinides and neodymium in NaCl, MgCl2, and CaCl2 solutions: Solubility, hydrolysis, and ternary Ca-M(III)-OH complexes, *Pure and Applied Chemistry 81*, 1555-1568.
[44] Tan, K. L., and Hameed, B. H. (2017) Insight into the adsorption kinetics models for the removal of contaminants from aqueous solutions, *J Taiwan Inst Chem E 74*, 25-48.
[45] Brewer, A., Chang, E., Park, D. M., Kou, T., Li, Y., Lammers, L. N., and Jiao, Y. (2019) Recovery of Rare Earth Elements from Geothermal Fluids through Bacterial Cell Surface Adsorption, *Environ. Sci. Technol. 53*, 7714-7723.
[46] Vander Hoogerstraete, T., Blanpain, B., Van Gerven, T., and Binnemans, K. (2014) From NdFeB magnets towards the rare-earth oxides: a recycling process consuming only oxalic acid, *RSC Advances 4*, 64099-64111.
[47] Hoffman, A. S. (2012) Hydrogels for biomedical applications, *Advanced Drug Delivery Reviews 64*, 18-23.
[48] Nguyen, K. T., and West, J. L. (2002) Photopolymerizable hydrogels for tissue engineering applications, *Biomaterials 23*, 4307-4314.
[49] D'Angelo, A. J., and Panzer, M. J. (2017) Enhanced Lithium Ion Transport in Poly(ethylene glycol) Diacrylate-Supported Solvate Ionogel Electrolytes via Chemically Cross-linked Ethylene Oxide Pathways, *The Journal of Physical Chemistry B 121*, 890-895.
[50] Watkins, A. W., and Anseth, K. S. (2005) Investigation of Molecular Transport and Distributions in Poly(ethylene glycol) Hydrogels with Confocal Laser Scanning Microscopy, *Macromolecules 38*, 1326-1334.
[51] Russell, R. J., Axel, A. C., Shields, K. L., and Pishko, M. V. (2001) Mass transfer in rapidly photopolymerized poly(ethylene glycol) hydrogels used for chemical sensing, *Polymer 42*, 4893-4901.
[52] Cruise, G. M., Scharp, D. S., and Hubbell, J. A. (1998) Characterization of permeability and network structure of interfacially photopolymerized poly(ethylene glycol) diacrylate hydrogels, *Biomaterials 19*, 1287-1294.
[53] Mellott, M. B., Searcy, K., and Pishko, M. V. (2001) Release of protein from highly cross-linked hydrogels of poly(ethylene glycol) diacrylate fabricated by UV polymerization, *Biomaterials 22*, 929-941.
[54] D'Angelo, P., Martelli, F., Spezia, R., Filipponi, A., and Denecke, M. A. (2013) Hydration Properties and Ionic Radii of Actinide(III) Ions in Aqueous Solution, *Inorg. Chem. 52*, 10318-10324.
[55] Müller, G. T. A., and Stokes, R. H. (1957) The mobility of the undissociated citric acid molecule in aqueous solution, *Transactions of the Faraday Society 53*, 642-645.
[56] Chu, K. H., and Hashim, M. A. (2007) Copper biosorption on immobilized seaweed biomass: Column breakthrough characteristics, *J Environ Sci-China 19*, 928-932.
[57] Hu, Q., Xie, Y., Feng, C., and Zhang, Z. (2019) Fractal-like kinetics of adsorption on heterogeneous surfaces in the fixed-bed column, *Chemical Engineering Journal 358*, 1471-1478.
[58] Yagub, M. T., Sen, T. K., Afroze, S., and Ang, H. M. (2015) Fixed-bed dynamic column adsorption study of methylene blue (MB) onto pine cone, *Desalin Water Treat 55*, 1026-1039.
[59] Jahangiri-rad, M., Jamshidi, A., Rafiee, M., and Nabizadeh, R. (2014) Adsorption performance of packed bed column for nitrate removal using PAN-oxime-nano Fe2O3, *J Environ Health Sci 12*, 90.
[60] Das, N., and Das, D. (2013) Recovery of rare earth metals through biosorption: An overview, *Journal of Rare Earths 31*, 933-943.
[61] Kucuker, M. A., Wieczorek, N., Kuchta, K., and Copty, N. K. (2017) Biosorption of neodymium on Chlorella vulgaris in aqueous solution obtained from hard disk drive magnets, *PLoS One 12*, e0175255.
[62] Hall, S., Cooke, M., Pacek, A. W., Kowalski, A. J., and Rothman, D. (2011) Scaling up of Silverson Rotor-Stator Mixers, *Can J Chem Eng 89*, 1040-1050.
[63] Florek, J., Giret, S., Juère, E., Larivière, D., and Kleitz, F. (2016) Functionalization of mesoporous materials for lanthanide and actinide extraction, *Dalton Transactions 45*, 14832-14854.
[64] Qi, D. (2018) Chapter 7 - Chemical Separation Method, In *Hydrometallurgy of Rare Earths* (Qi, D., Ed.), pp 671-741, Elsevier.
[65] Kim, D., Powell, L. E., Delmau, L. H., Peterson, E. S., Herchenroeder, J., and Bhave, R. R. (2015) Selective Extraction of Rare Earth Elements from Permanent Magnet Scraps with Membrane Solvent Extraction, *Environ. Sci. Technol. 49*, 9452-9459.
[66] Diaz, L. A., and Lister, T. E. (2018) Economic evaluation of an electrochemical process for the recovery of metals from electronic waste, *Waste Management 74*, 384-392.
[67] Jin, H., Park, D. M., Gupta, M., Brewer, A. W., Ho, L., Singer, S. L., Bourcier, W. L., Woods, S., Reed, D. W., Lammers, L. N., Sutherland, J. W., and Jiao, Y. (2017) Techno-economic Assessment for Integrating Biosorption into Rare Earth Recovery Process, *ACS Sustainable Chemistry & Engineering 5*, 10148-10155.
[68] Ku, H. H. (1966) Notes on the use of propagation of error formulas, *Journal of Research of the National Bureau of Standards — C. Engineering and Instrumentation 70C*, 263-273.